AIChE

Modeling of Heat Recovery from a Steam-Gas Mixture in a High-Temperature Sorption Process

Kwangkook Jeong
Dept. of Mechanical Engineering, Arkansas State University, Jonesboro, AR 72467

Shivaji Sircar and Hugo S. Caram
Dept. of Chemical Engineering, Lehigh University, Bethlehem, PA 18015

DOI 10.1002/aic.12564
Published online March 22, 2011 in Wiley Online Library (wileyonlinelibrary.com).

A high pressure condenser is considered to remove water vapor as well as recover heat from the desorbed steam—CO_2 gas mixture in a novel sorption enhanced reaction process. It is possible to have water condensation at the gas side as well as water evaporation at the coolant water side because of large temperature difference between the hot and cold side. A model of heat and mass transfer and phase change was developed to understand the complex phenomena associated with the simultaneous condensation and evaporation taking place in the unit. A finite difference method was used to solve the boundary value problem. Additional insight was obtained by describing the operating lines and equilibrium condition in an enthalpy diagram. The model was used to explore the performance in terms of the heat recovery. The heat recovery was best at the beginning of the process when the superheated steam was generated. © 2011 American Institute of Chemical Engineers *AIChE J,* 58: 312–321, 2012
Keywords: condensation, evaporation, heat transfer, mass transfer, energy

Introduction

Conventional production of hydrogen from coal gasification is a commercial technology. As shown in Figure 1, it involves high pressure partial oxidation of coal with oxygen and steam to produce a synthesis gas containing H_2, CO, CO_2, H_2O, and trace amounts of H_2S and COS. The synthesis gas is cooled down and the impurities are removed. Then the gas is subjected to catalytic water gas shift (WGS) reaction ($CO + H_2O \leftrightarrow CO_2 + H_2$) for converting most of the H_2O to H_2. The effluent gas from WGS reactor is sent to a gas purification system for production of pure H_2 through a condensation separation process and a pressure swing adsorption process.[1]

Correspondence concerning this article should be addressed to K. Jeong at kjeong@astate.edu

In this study, a novel TSSER (Thermal Swing Sorption Enhanced Reaction) process has been developed to combine the water gas shift reaction and the subsequent CO_2 separation from the reaction product in a single unit operation for simultaneous production of essentially pure CO_2 and H_2 products, both at feed gas pressures (Figure 2). A H_2 enriched product ($\sim$99.99 + %) is produced at feed pressure by condensing out the water from the reactor effluent by cooling. Then the sorber-reactor is counter-currently purged with superheated steam at pressure P_H and temperature T_H until most of the CO_2 is desorbed out of the column.

A high pressure condenser is used to condense the steam from the desorbed gas mixture and produce nearly pure carbon dioxide at the reactor pressure. In this work, a heat exchanger model is used to determine the best heat recovery through case studies in the process.[2]

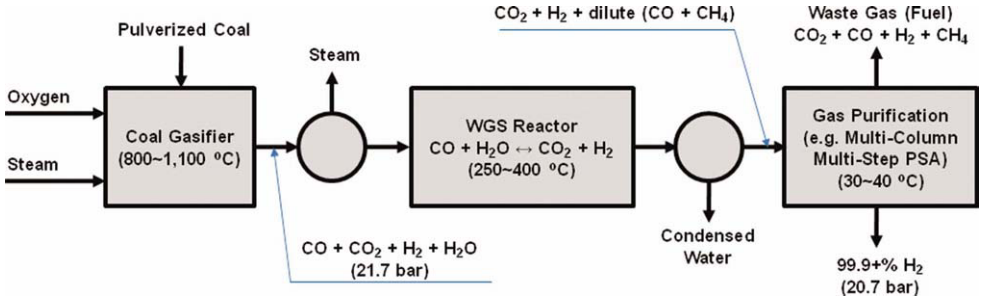

Figure 1. Schematic of conventional H_2 production system from coal gasification.[1]

[Color figure can be viewed in the online issue, which is available at wileyonlinelibrary.com.]

It is necessary for condensation modeling to consider the effect of the non-condensable CO_2 gas exhausted with the purge steam from the TSSER condensation process. The condenser is operated at high pressure up to 40 bar on both sides with large temperature differences (up to 170°C in terms of LMTD) between the hot and cold side. Accordingly, it is important to predict properties at high pressure and post dryout heat transfer in doing boiling modeling.

Previous Work on Condensation Heat Transfer

In 1980, Webb et al.[3] developed a one-dimensional numerical model to predict condensation with the effect of non-condensable gases in a 10-row by 10-column finned tube heat exchanger by solving the Colburn-Hougen equation for refrigerant R-11 and air mixture. An iterative solution procedure was applied to solve the equation.

From 1999 to 2003, Osakabe et al.[4–7] carried out one-dimensional heat and mass balance calculations for the condensation of flue gas in bare and finned tube heat exchangers. Experimental studies using actual flue gas from propane, natural gas, and oil combustion were conducted to investigate the effect of parameters and then compared with the computational results.

In 2005, Oh et al.[8–10] performed steam condensation experiments inside vertical tube submerged in pool water for complete condensation, cyclic venting, and through-flow modes. With pressure ranging from 0.1 to 0.4 MPa, their results showed that as the system pressure increased, the condensation heat transfer rate was enhanced but the condensation heat transfer coefficient decreased.

In 2008, Lee et al.[11] developed a theoretical model using a heat and mass transfer analogy and a simple model using Lee and Kim's correlation were developed to investigate the effects of noncondensable gas on steam condensation heat transfer inside a vertical submerged in pool water and applied to the design of a passive residual heat removal system (PRHRS) condensation heat exchanger in a SMART-P plant. They investigated the effects of the system pressure on the PRHRS condensation heat exchanger. The phase-change region to complete condensation of steam at the given system became shorter as the system pressure increased from 1.3 to 8.6 MPa because of enhanced heat transfer.

In 2010, Jeong et al.[12,13] derived energy balance equations governing heat and mass transfer in condensing heat exchanger designed for separating water vapor and sulfuric acid from flue gas of power plant. A computer program was developed to solve the split boundary problem with the equations by using one dimensional finite difference method. The modeling results were verified with test results made in power plant and showed good agreement.

Previous Work on Boiling Heat Transfer at High Pressure

In 1962, Schrock et al.[14] developed an empirical correlation to predict local heat transfer coefficients for forced flow boiling of water in vertical tubes at pressures ranging from 2.9 to 34.8 bar, which was recommended for the range of quality from 0 to 50%.

In 2000, Mori et al. classified their dryout results into three characteristic regimes based on the experimental trends they observed and presented prediction methods for their values of dryout inception x_{di} and completion x_{de}.

In 2005, experimental data taken by Wojtan et al.[15,16] agreed with dryout regime of Mori et al.[17] The approach of Mori et al. was been extended by including the heat flux effect using the non-dimensional ratio and new empirical factors based on all experimental points and using the least square method.

Analytical Modeling

In this study, the governing equations based on mass and energy balances for water boiling and condensation were derived to predict the gas exit temperature, water condensation rate, and mole fraction at the gas side and cooling water exit temperature, steam generation rate, and quality at the coolant side.

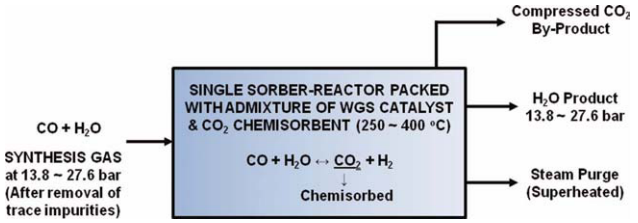

Figure 2. Schematic of TSSER for simultaneous H_2 and CO_2 production system.[2]

[Color figure can be viewed in the online issue, which is available at wileyonlinelibrary.com.]

Further insight into the model was obtained using a graphical method that illustrates the operating conditions and bounds in the process. As part of the study, several cases were analyzed for evaluation of the system.

Mass and Energy Balances

If there is no condensation in the gas side or evaporation in the coolant side, the energy equations for both streams are the familiar:

$$\dot{m}_g \cdot c_{p.g} \cdot \frac{dT_g}{dA} = h_g \cdot (T_g - T_w) \quad (1)$$

$$\dot{m}_c \cdot c_{p.c} \cdot \frac{dT_c}{dA} = h_c \cdot (T_w - T_c) \quad (2)$$

where the gas and wall temperatures can be found by using Eqs. 1 and 2, respectively. In this case, both $\dot{m}_g$ and $\dot{m}_c$ remain constant because of no mass transfer.

If there is condensation in the gas side, the gas temperature can be found from the modified equation of Eq. 1, at which wall temperature (T_w) is replaced with the interfacial temperature (T_i), as the tube wall is assumed to be covered by condensed liquid film. The wall temperature still can be found from Eq. 2 as there is no change at the control volume. The interfacial temperature can be found by the well known Colburn-Hougen relation:

$$h_g(T_g - T_i) + k_m \cdot l_{LC} \cdot (y_{H_2O} - y_i) = h_c(T_i - T_c) \quad (3)$$

Because of condensation, mass flow in the gas side is no longer constant and it varies according to the relation:

$$\frac{d\dot{m}_g}{dA} = k_m \cdot (y_{H_2O} - y_i) \quad (4)$$

If there is evaporation in the coolant side, the temperature will remain constant at the boiling point of the coolant and the mass of vapor will vary as

$$\frac{d\dot{m}_{bo}}{dA} = \frac{h_g(T_g - T_w)}{l_{LV}} \quad (5)$$

In all cases, the thermal resistance of the material has been ignored.

Heat and Mass Transfer Coefficients

The Colburn j factors for heat and mass transfer with their applicable ranges are defined as[18,19]:

$$j_H = St \cdot P_r^{\frac{2}{3}} = \frac{h}{\rho \cdot c_p \cdot V} P_r^{\frac{2}{3}} \quad 0.6 < P_r < 60 \quad (6)$$

$$j_m = St_m \cdot Sc^{\frac{2}{3}} = \frac{k_D}{V} Sc^{\frac{2}{3}} \quad 0.6 < Sc < 3,000 \quad (7)$$

where h is convective heat transfer coefficient [W/m^2·K] and k_D is convective mass transfer coefficient [m/s]. The Chilton-Colburn analogy requires equating Eqs. 6 and 7, that is, $j_H = j_m$. Then an expression for the mass transfer coefficient, k_m, is derived as:

$$k_m = \frac{h_g \cdot M_{H_2O}}{c_{p,g} \cdot M_g \cdot y_{lm} \cdot Le_{H_2O-gas}^{2/3}} \quad (8)$$

All properties are calculated based on composition of mixture, and y_{lm}, the logarithmic mole fraction of the non-condensable gas across the film[20,21] is:

$$y_{lm} = \frac{y_{ni} - y_{nb}}{\ln(y_{ni}/y_{nb})} \quad (9)$$

where y_{ni} and y_{nb} are the mole fractions of non-condensable gases at the gas/film interface and in the bulk flow, respectively.

The variable Le_{H_2O-gas} at Eq. 8 is the Lewis number of water vapor in the desorption gas, in which D_{H_2O-gas} is the mass diffusion coefficient of water vapor in the desorption gas.[21]

$$Le_{H_2O-gas} = \frac{Sc}{Pr} = \frac{\alpha_g}{D_{H_2O-gas}} \quad (10)$$

Convective Heat Transfer Coefficient for the Gas Side

To predict the convective heat transfer coefficient on the gas side of a bare tube bank, an empirical correlation proposed by Zukauskas,[22] Eq. 11, is used.

$$\overline{Nu}_D = 0.021 \cdot Re_{D,max}^{0.84} \cdot Pr^{0.36} \cdot \left(\frac{Pr}{Pr_s}\right)^{1/4} \quad (11)$$

Convective Heat Transfer Coefficient Inside Coolant Tubes

The single phase flow heat transfer coefficient of cooling water side inside tube is predicted by using the Gnielinski's correlation,[23] Eq. 12 is valid for either pure liquid or pure vapor.

$$Nu_D = \frac{\left(\frac{f}{8}\right)(Re_D - 1000)Pr}{1 + 12.7\left(\frac{f}{8}\right)^{\frac{1}{2}}(Pr^{2/3} - 1)} \quad (12)$$

Boiling Heat Transfer Coefficient Inside Coolant Tubes

However, as the tube wall temperature exceeds the saturation temperature of the liquid, boiling starts at the wall. With the start of flow boiling, the coolant water side changes to two phase flow of vapor and liquid. The boiling heat transfer coefficient (h_{bo}) should be used to predict the boiling heat transfer inside the tube. The boiling heat transfer coefficient is calculated by using Schrock-Grossman correlation,[14,24] Eq. 13, which can be applicable for the high pressure range.

$$h_{bo} = 0.739 \cdot [B_o \times 10^4 + 1.5(1/\chi_{tt})^{2/3}] \cdot h_l \quad (13)$$

where h_l is single phase pure liquid heat transfer coefficient evaluated from Eq. 12. The variables B_o and χ_{tt} are the boiling number used by Mumm and the Lockhart-Martinelli parameter, respectively, defined as

$$B_o = \frac{Q_c^*}{G \cdot l_c} \tag{14}$$

$$1/\chi_{tt} = \{x/(1-x)\}^{0.9}(\rho_l/\rho_v)^{0.5}(\mu_v/\mu_l)^{0.1} \tag{15}$$

where G and x are mass flow per unit area and quality, respectively. ρ and μ are density and viscosity, respectively. Subscripts of l and v denote liquid and vapor phase, respectively.

Post Dryout Heat Transfer

The operational conditions for the system call for high pressure (40 bar) and large temperature differences (LMTD = 170°C). The large temperature difference between hot and cold side entails a large temperature gap (wall superheat = 70°C) between the tube wall and the water to be boiled, which can cause a serious instability of two phase flow and unpredictable transition to dry out. The prediction for the dryout point and the post-dryout heat transfer is critical for the modeling of boiling because the dryout point can occur earlier because of the large temperature difference. The inception and completion of dryout can be calculated from the following equations[15,16]:

$$x_{di} = 0.58\, e^{[0.52-0.235 \cdot W\, e_V^{0.17} Fr_V^{0.37} (\frac{\rho_V}{\rho_L})^{0.25}]} \tag{16}$$

$$x_{do} = 0.61\, e^{[0.57-5.8 \cdot 10^{-3} \cdot W\, e_V^{0.33} Fr_V^{0.15} (\frac{\rho_V}{\rho_L})^{-0.09}]} \tag{17}$$

Assumptions and Simplifications

The following assumptions were made to complete the development of modeling in this study. It is assumed that the boiling heat transfer coefficient is linear from the inception to the completion point of dryout. Only film condensation is assumed on the tube wall surface. The thermal resistance between the liquid film and the tube wall is neglected. There is no heat loss from the system to the environment. The coolant is pure water while the desorption gas is a mixture of steam and CO_2.

Numerical scheme

The governing equations corresponding to a split boundary value problem are solved using an iterative numerical scheme and a one dimensional finite difference method (FDM) with forward differencing. The known variables were: inlet gas temperature, flow rate and mole fraction of steam, inlet cooling water temperature, and flow rate. The condenser area and configuration are fixed. The model will yield the exit gas temperature, steam mole fraction and temperature of coolant and condensation rate of steam at gas side. All properties at high pressure were predicted by using the database from National Institute of Standards and Technology (NIST).[25]

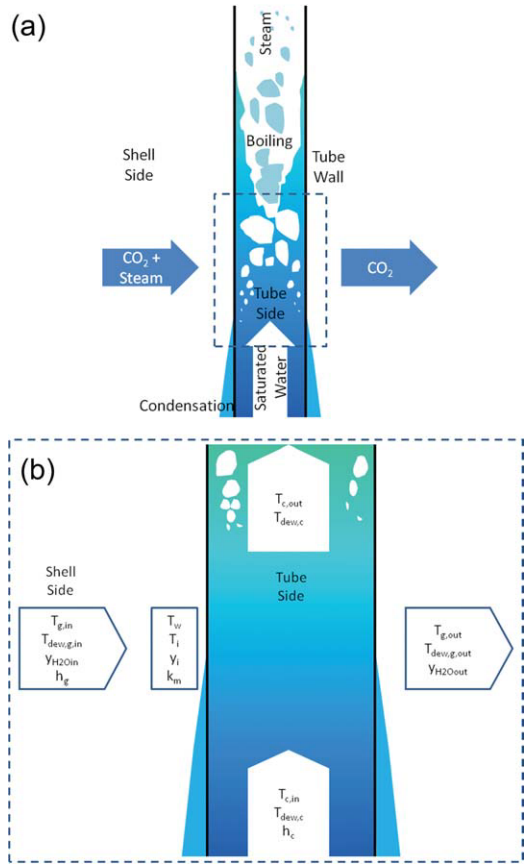

Figure 3. Schematic of (a) control volume in heat exchanger and (b) main variables.

[Color figure can be viewed in the online issue, which is available at wileyonlinelibrary.com.]

The condenser operates with the desorption gas (CO_2 + Steam) in the shell side and the cooling water in the tubes. Figure 3a illustrates a simplified schematic of the control volume of a finite difference element in the heat exchanger. Flow appears cross flow to the tubes, but the overall flow pattern in the equipment is counter flow. Heat and mass transfer for water condensation in the shell side and phase change for flow boiling in the tube side are considered within this control volume.

Figure 3b shows the main variables to be considered for the modeling. The desorption gas temperatures at the inlet and outlet of the shell side are expressed as $T_{g,in}$ and $T_{g,out}$, respectively. The saturation temperatures corresponding to steam partial pressures at the inlet ($y_{H_2O,in}$) and outlet ($y_{H_2O,out}$) of gas side are $T_{sat,g,in}$ and $T_{sat,g,out}$, respectively. The variables $T_{c,in}$ and $T_{c,out}$ express cooling water temperatures at the inlet and outlet of the tube side, respectively. The saturation temperature corresponding to the operating pressure at the cooling water side is $T_{sat,c}$. The tube wall temperature is T_w. The variable T_i is the interfacial temperature at shell side which is the saturation temperature corresponding to the interfacial mole fraction of steam at the liquid–vapor interface film. The heat transfer coefficients for the gas and cooling water side are h_g and h_c, respectively. The mass transfer coefficient for the case of condensation is k_m.

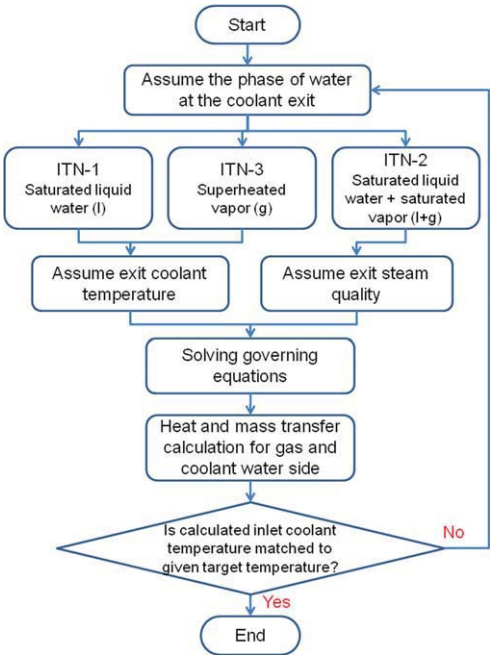

Figure 4. Schematic of numerical scheme for modeling.

[Color figure can be viewed in the online issue, which is available at wileyonlinelibrary.com.]

To apply the FDM method, total surface area of the entire system was discretized into a large number of cells. Governing equations are solved at each cell to solve unknown variables from the inlet of gas side to the exit of gas side.

As shown in Figure 4, there are three possibilities for the coolant condition at the exit: liquid, saturated liquid and vapor and superheated vapor. The actual condition is obtained by iteration by assuming an exit condition for the coolant, integrating backwards to match the feed condition of the coolant at the entrance of the condenser tube side. Three loops are used to iterate on those possible exit conditions.

The first loop (ITN-1) assumes no evaporation ($x = 0$) at the coolant exit and iterates on the exit coolant temperature until the calculated inlet cooling water temperature approaches the correct inlet value. The ITN-1 calculates the condensation rate on the gas side without evaporation on the tube side. During the loop, tube wall temperature stays below the saturation temperature at both sides everywhere in the heat exchanger. In this loop, the assumed variable is only the cooling water exit temperature.

If the coolant leaves the condenser as a liquid vapor mixture, the iteration (ITN-2) is carried out on the mass fraction of steam at the coolant exit. The program calculates phase changes for the cases that the tube wall temperature is either (1) higher or (2) lower than saturation temperature. So it allows both boiling at coolant side and condensation at gas side. Most commonly, it finds boiling near the exit of coolant side and condensation near the exit of gas side. The program converges if the calculated cooling water inlet temperature reaches to the target temperature with the assumed steam quality for the range of $0 < x < 1.0$. The assumed variable is only the steam quality at the coolant exit as the exit coolant temperature is assumed to be the saturation temperature.

If the coolant leaves as superheated steam ($x = 1$), the third loop (ITN-3) begins with an assumption of exit superheated steam temperature. The ITN-3 computes the phase change from the saturated liquid phase to the superheated steam on the coolant tube side with a possibility of condensation on the gas side. The program can be completed if the calculated cooling water inlet temperature reaches to the target temperature with the assumed exit superheated steam temperature.

Process conditions

For the study, a counter-flow shell and tube heat exchanger with an inside diameter of 0.6 m, length of 6 m, and 2 vanes per meter of shell length and 612 tubes of 12.7 mm OD and 3 mm thickness was used in the study. The tube pitch was 1.5 (s_L/d_o, longitudinal) $\times$ 1.5 (s_T/d_o, transverse), and total heat transfer area of 224 m^2. The composition of the stripping gas changes during the desorption process as the mass flow of CO_2 decreases as it is removed from the bed. As the desorption progresses, the mole fraction of CO_2 at the gas inlet of heat exchanger varies from 1.0 to zero. As shown in Table 1, the CO_2 concentration varies from 99.0 to 1.35%, where as the molar flow rate of CO_2 decreases from 3.57 to 0.05 kmol/s during the desorption cycle. The coolant side is assumed to be a sub-cooled liquid phase at the inlet and increase its flow rate from 1.34 to 7.57 kmol/s and lower its inlet temperature from 240 to 200°C to reach higher condensation efficiency. Figure 5 shows the CO_2 mole fractions and total flow rates in the gas side during the desorption process. The values used in the analysis were selected from the results of recent simulation done by our research group, at which the pseudo state behavior was assumed in terms of snapshot of the process.

Graphical method using bounded constraint diagram

As multiple phases are possible, further insight into the process can be obtained by using a graphical method to

Table 1. Boundary Conditions for Modeling

				Molar Flow Rate			
	Pressure (bar)	Inlet Temperature (°C)	Species	Case I	Case II	Case III	Case IV
Gas side	40	550	CO_2 (kmol/s)	3.57	3.80	0.37	0.05
			H_2O (g) (kmol/s)	0.04	0.48	3.60	3.66
			Total (kmol/s)	3.61	4.28	3.97	3.71
			yCO_2 (vol %)	99.0	89.0	9.32	1.35
Coolant side	40	200–240	H_2O (l) (kmol/s)	1.34	2.93	9.0	7.57
		Inlet temperature (°C)		240	240	200	200

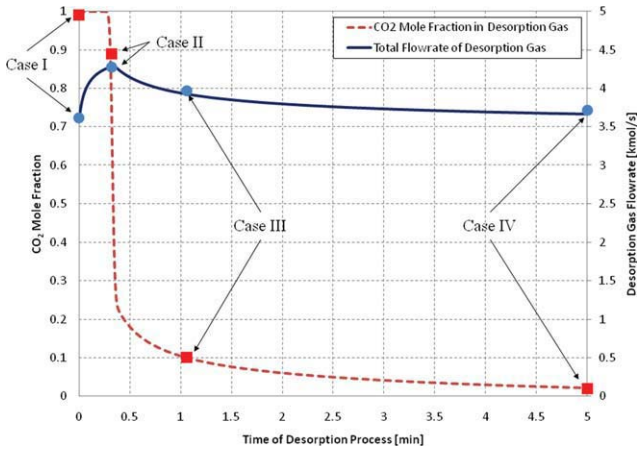

Figure 5. Variations of CO_2 mole fractions and total flow rates during the desorption cycle.

[Color figure can be viewed in the online issue, which is available at wileyonlinelibrary.com.]

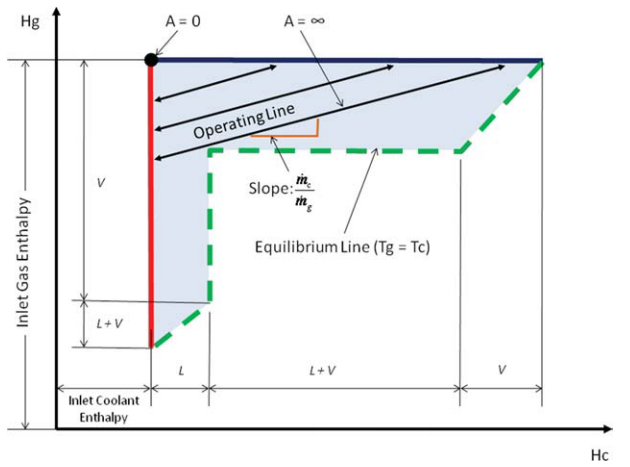

Figure 7. Schematic of bounded constraint diagram.

[Color figure can be viewed in the online issue, which is available at wileyonlinelibrary.com.]

study the operational limits of the condenser unit described above. The control volume defined in Figure 6 which consists of the upper hot desorption gas side and lower coolant water side is used to carry out an enthalpy balance. Mixture gas of $\dot{m}_g$ (CO_2 and H_2O) enters into the gas side and exits with condensed liquid water and CO_2, while cooling water enters at liquid phase into the coolant side and may exit as either liquid or vapor or a mixture of both. Variables of enthalpies for gas and coolant side passing the dashed volume are expressed by H_g and H_c, respectively.

The enthalpies entering and exiting the volume are shown at the left and right side of Eq. 18, respectively. The enthalpy balance yields a linear operating line connecting the enthalpies of the gas phase and the coolant, when the enthalpy of the gas phase is given per unit of mass (mole) of non-condensable CO_2.

$$\dot{m}_g \cdot H_g + \dot{m}_c \cdot H_{cl} = \dot{m}_g \cdot H_{go} + \dot{m}_c \cdot H_c \tag{18}$$

$$H_g = \frac{\dot{m}_c}{\dot{m}_g} \cdot (H_c - H_{cl}) + H_{go} \tag{19}$$

As shown in Figure 7, the operating line for the condenser in the (H_g, H_c) plane is constrained in the region bounded by the following lines: (1) a vertical line corresponding to the enthalpy of the inlet cooling water, (2) a horizontal line corresponding to the enthalpy of the inlet gas, and (3) an equilibrium line corresponding to equal temperature of the gas and cooling water side. The enthalpy lines taken from the inlet cooling water and inlet gas temperature can be drawn by the given boundary conditions at each inlet. The isotherm enthalpy line is drawn by the assumption that the cooling water temperature is the same as the gas at any arbitrary points. With those three enthalpy lines, a bounded constraint diagram can be established in the (H_g, H_c) plane mapped from the temperature domain. Then the straight line made by the result of modeling, which is called "operating line," is verified by checking if the line is placed inside the bounded graph without crossing or passing the bounded lines.

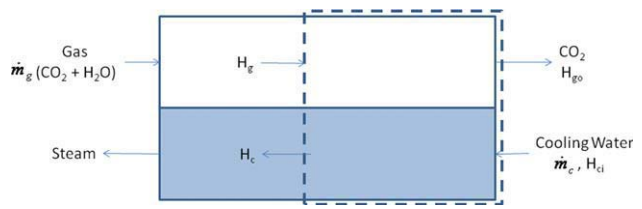

Figure 6. Control volume for bounded constraint diagram.

[Color figure can be viewed in the online issue, which is available at wileyonlinelibrary.com.]

The actual position of the line depends on the heat transfer area available (A) and it shifts from a single point for $A = 0$ to a line tangential to the equilibrium point for an infinite area. The slope of the operating line depends on the flow rate ratio of the coolant to gas, $\frac{\dot{m}_c}{\dot{m}_g}$, as shown in Eq. 19. Figure 7 contains distinct sections named L (liquid), $L+V$ (liquid and vapor), and V (vapor) to clearly explain the phase matching to each section of the line.

Figure 8 shows all four cases given in Table 1. As shown in Figure 8a, the enthalpies of coolant and vapor phase (H_c and H_g) are contained, again, in an area bound by three lines: a horizontal line for the inlet gas enthalpy, a vertical line of the inlet cooling water enthalpy and an "equilibrium" line corresponding to equal gas and coolant temperature. With Figure 8a for Case I, which is saturated water being fed into the system, it is seen that the far right end of the operating line is located above the vapor phase of cooling water side of the isotherm enthalpy line, which agrees with the modeling result that has superheated vapor at the exit of cooling water side. Moving from Figure 8a of Case I to Figure 8d of Case IV, the slope ($\frac{\dot{m}_c}{\dot{m}_g}$) of the operating line increases as the mass flows of gas decrease and coolant side increase. Figure 8d shows that the operating line has a very steep slope because of very large ratio of $\frac{\dot{m}_c}{\dot{m}_g}$ at the end of process. It means that all vapor involved at the gas side is removed by condensation because of much higher heat transfer to the coolant side with higher flow rate ratio of cooling

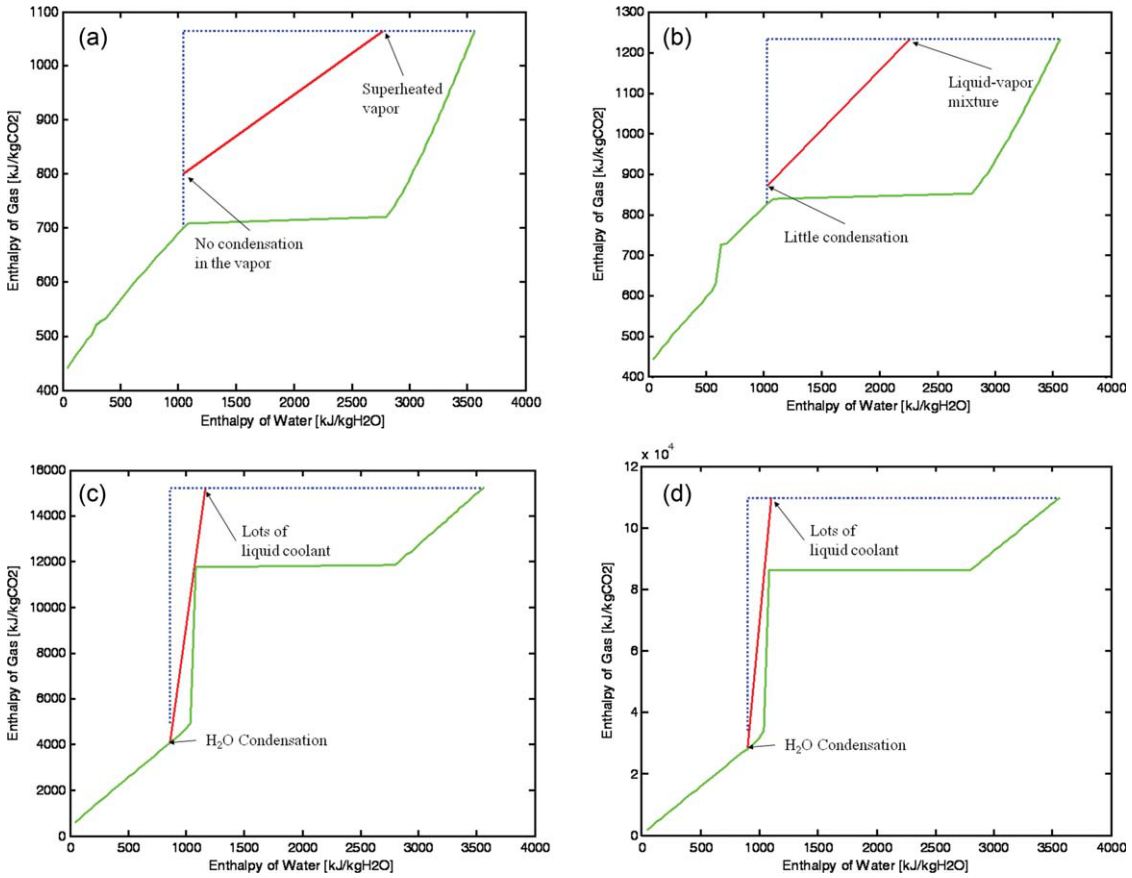

Figure 8. Verifications of modeling results using the bounded constraint diagram for (a) Case I, (b) Case II, (c) Case III, and (d) Case IV.

[Color figure can be viewed in the online issue, which is available at wileyonlinelibrary.com.]

water to gas side. Notice that the operating lines do not intersect the equilibrium lines.

Results and Discussion

The simulation of a high pressure condenser has been carried out for a pilot scale shell and tube heat exchanger but can be extended to any scale. The cross-counter flow heat exchanger has the desorption gas flowing into the shell side and coolant water flowing into the tube side. The heat exchanger operated at high pressure of 40 bar has been targeted (1) to remove steam from the desorption gas in the shell side and (2) to produce steam in the tube side to recover heat from the hot gas side.

Figure 9 shows the profiles of gas temperature, tube wall temperature, and cooling water temperature as results of all cases shown at Table 1. As shown in Figure 9a, it is seen that the cooling water leaves the condenser as superheated steam. It is seen that the tube wall temperature abruptly increases at halfway of the heat transfer area because of the onset of post-dryout heat transfer. At the post-dryout region, the liquid film may dry out or becoming entrained in the high velocity vapor-phase, which results in poor heat transfer. In the other extreme case, Figure 9d shows that water condensation occurs at over all heat transfer surface area as the gas side gets cooled enough because of relatively high ratio of $\frac{\dot{m}_c}{\dot{m}_g}$. Each result of modeling in Figures 9a–d matches well with the results of bounded constraint diagram in Figures 8a–d.

Figure 10 shows the exit quality of coolant tube side during the time of desorption cycle. Quality is defined as the mass percentage of water vapor to total coolant flow rate in the tube side. The quality at the coolant exit produces 100% steam in the initial stage of the process as the coolant side of relatively small flow rate gets high enough heat transfer to be converted to superheat. Hundred percent of quality means that all saturated liquid phase coolant water is evaporated into fully saturated vapor phase. However, at the end of the cycle, the quality decreases to zero because of the increased coolant flow rate so that it can condense the desorbed gas.

Figure 11 shows condensation efficiency at the gas side. Condensation efficiency is defined as the fraction of incoming steam condensed. For example, 100% of condensation efficiency means all incoming vapor at gas side is condensed to liquid phase at the exit. The higher condensation efficiency means the higher removal efficiency of steam from the desorption gas mixture. The condensation efficiency increases from 0 to 98.7% to capture water vapor in the desorption gas by increasing the coolant flow rate and lowering its temperature.

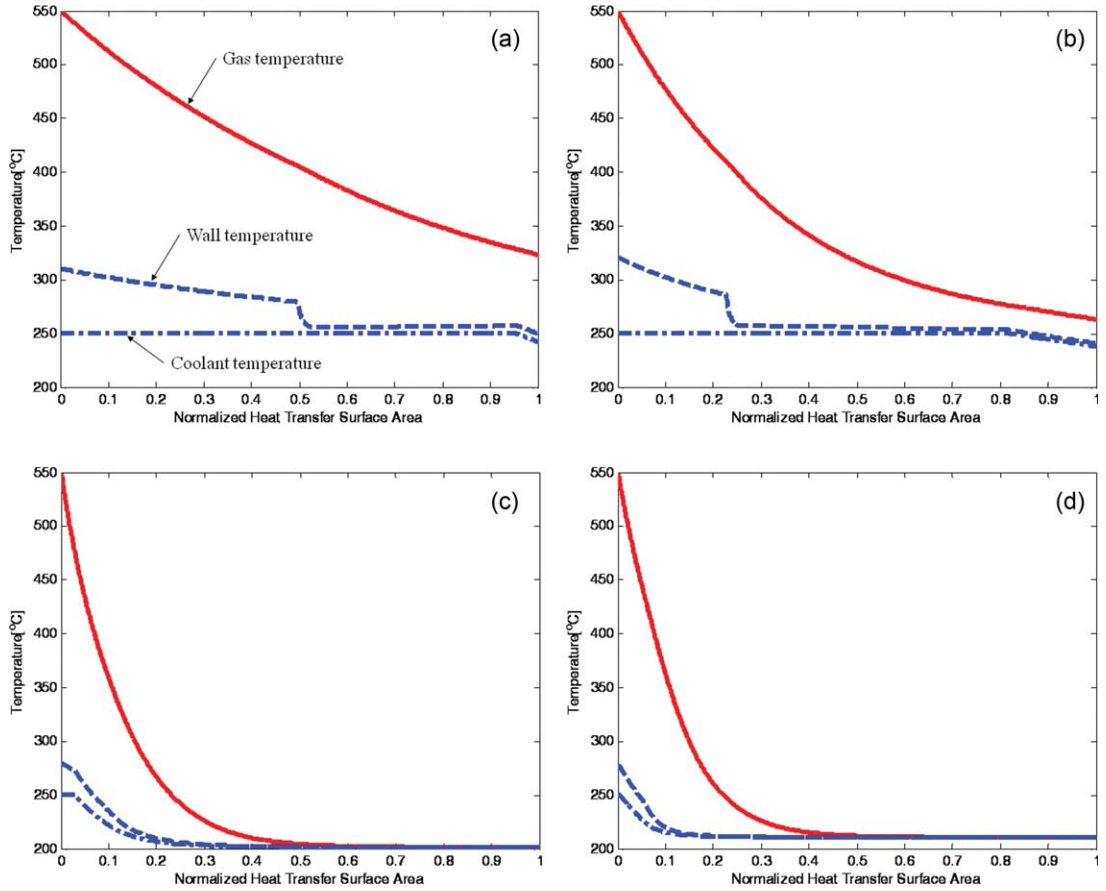

Figure 9. Temperature profiles as results of modeling for (a) Case I, (b) Case II, (c) Case III, and (d) Case IV.

[Color figure can be viewed in the online issue, which is available at wileyonlinelibrary.com.]

Figure 12 shows the heat recovery rate during the desorption cycle. The heat recovery rate is defined as the ratio of the enthalpy change in gas side to the enthalpy of incoming gas using the enthalpy of the entering cooling water as a reference. It varies from 11.3 to 32.0% during the cycle and shows a peak at 0.3 min as is also seen at the pattern of desorption gas flow rate in Figure 5. To achieve 100% of steam quality, the coolant water should be decreased but this will reduce the condensation in the gas side. For a 100% steam removal, a high flow rate of coolant relative to gas side is needed but it will be disadvantageous for coolant tube side's steam generation, which is trade-off with the case of steam generation. The higher heat recovery profile occurred under steam generation in the coolant side.

Conclusions

The design of a high pressure condenser has been studied for heat recovery from a gas-steam mixture. A possible application is Temperature Swing Sorption Enhanced Reaction (TSSER) process, where steam is removed from CO_2 stream generated during the coal gasification process.

The condenser is modeled by a combination of two differential equations with split boundary conditions and a nonlinear algebraic equation for the interfacial temperature. A numerical scheme was made by using an iterative numerical scheme and a one dimensional finite difference method (FDM) with forward differencing.

Process conditions for modeling of case studies were taken with variable flow rates of CO_2 and steam during desorption cycle. A graphical method was also presented by

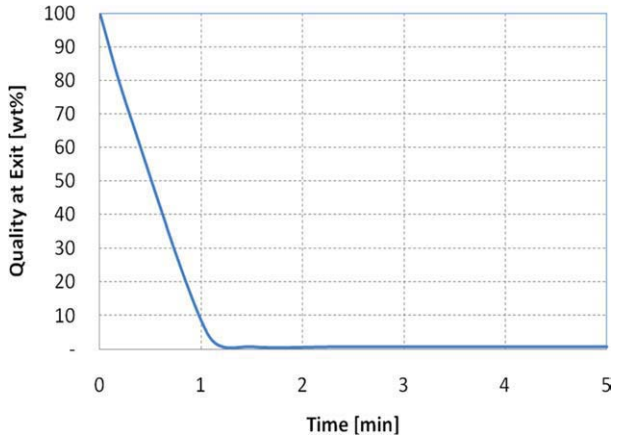

Figure 10. Steam quality at the coolant exit during the desorption cycle.

[Color figure can be viewed in the online issue, which is available at wileyonlinelibrary.com.]

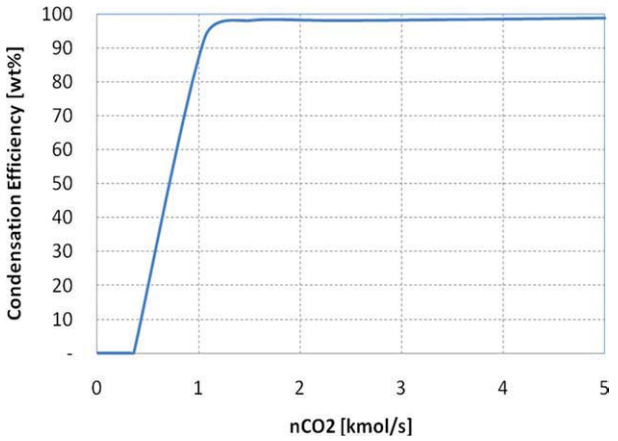

Figure 11. Condensation efficiency during the desorption cycle.

[Color figure can be viewed in the online issue, which is available at wileyonlinelibrary.com.]

Figure 12. Heat recovery rate during the desorption cycle.

[Color figure can be viewed in the online issue, which is available at wileyonlinelibrary.com.]

using a bounded constraint diagram which was made by three lines: lines of inlet coolant enthalpy, inlet gas enthalpy, and equilibrium temperature. The results of the numerical simulation match well the graphical method of the bounded constraint diagram.

Predicted heat recovery rates from the desorption gas side to the cooling water side ranged from 11.3 to 32%. The heat recovered was best occurred at the beginning of the process when superheated steam was generated.

Acknowledgments

The authors thank Prof. John Chen of Lehigh University, for his assistance with the boiling modeling and post dryout heat transfer.

Notation

A = heat transfer surface area
B_o = boiling number
c_p = specific heat
D = binary mass diffusivity
d = tube diameter
Fr = Froude number
f = friction factor
G = mass flow per unit area
H = enthalpy
H_{ci} = enthalpy at coolant inlet
H_{go} = enthalpy at gas exit
h = convective heat transfer coefficient
j = Colburn j factor
k_D = convective mass transfer coefficient
k_m = mass transfer coefficient
Le = Lewis number
l = latent heat
M = molecular weight
$\dot{m}$ = mass flow rate
$\underline{Nu}_D$ = local Nusselt number
$\overline{Nu}_D$ = average Nusselt number
n = mole
P_H = operating pressure
Pr = Prandtl number
Q = heat transfer rate
Q'' = heat transfer rate per unit area
Re_D = Reynolds number
S_c = Schmidt number
S_T = Stanton number
s_L = longitudinal distance between tubes
s_T = transverse distance between tubes
T = temperature
T_H = operating temperature
V = velocity
W_e = Weber number
X = quality
Y = mole fraction

Greek letters

α = thermal diffusivity
η = efficiency
λ = thermal conductivity
ρ = density
χ_{tt} = Martinelli parameter
σ = surface tension
μ = Viscosity

Subscripts

bo = boiling
c = cooling water side
sat = saturation
di = inception of dryout
do = completion of dryout
eff = effective
f = liquid film
g or gas = desorption gas
H_2O = water
i = interfacial
in = inlet
l = liquid phase
lm = log mean difference
LC = latent heat of condensation
LV = latent heat of vaporization
m = mass transfer
nb = non-condensable at bulk
ni = non-condensable at interface
out = outlet
v = vapor phase
w = tube wall

Literature Cited

1. Lee KB, Beaver MG, Caram HS, Sircar S. Reversible chemisorptions of carbon dioxide: simultaneous production of fuel-cell grade H2 and compressed CO2 from synthesis gas. *Adsorption*. 2007; 13:385–397.

2. Lee KB, Beaver MG, Caram HS, Sircar S. Performance of Na2O promoted alumina as CO2 chemisorbent in sorption-enhanced reaction process for simultaneous production of fuel-cell grade H2 and compressed CO2 from synthesis gas. *J Power Sources*. 2007;176:312–319.
3. Webb RL, Wanniarachchi AS. The effect of noncondensible gases in water chiller condensers—literature survey and theoretical predictions. *ASHRAE Trans*. 1980;80:142–159.
4. Osakabe M, Itoh T, Yagi K. Condensation heat transfer of actual flue gas on horizontal tubes. In: Proceedings of the 5th ASME/JSME Joint Thermal Engineering Conference, San Diego, CA 1999.
5. Osakabe M. Thermal-hydraulic behavior and prediction of heat exchanger for latent heat recovery of exhaust flue gas. *Proc ASME Heat Transfer Div*. 1999;2:43–50.
6. Osakabe M. Latent heat recovery from oxygen-combustion flue gas. *Energy Conversion Eng Conf Exhibit*. 2000;2:804–812.
7. Osakabe M, Yagi K, Itoh T, Ohmasa K. Condensation heat transfer on tubes in actual flue gas (parametric study for condensation behavior). *Heat Transfer Asian Res*. 2003;32:153–166.
8. Oh S, Revankar ST. Investigation of the noncondensable effect and the operational modes of the passive condenser system. *Nucl Technol*. 2005;152:71–86.
9. Oh S, Revankar ST. Effect of noncondensable gas in a vertical tube condenser. *Nucl Eng Des*. 2005;235:1699–1712.
10. Oh S, Revankar ST. Complete condensation in a vertical tube passive condenser. *Int Commun Heat Mass Transfer*. 2005;32:593–602.
11. Lee K, Kim MH. Modeling of condensation heat transfer for a PRHRS heat exchanger in a SMART-P plant. *Nucl Eng Des*. 2008;238:3252–3262.
12. Jeong K. Condensation of water vapor and sulfuric acid vapor in boiler flue gas. PhD. Dissertation, ProQuest, Lehigh University: Bethlehem, PA, 2009 ISBN # 9781109121285.
13. Jeong K, Kessen M, Bilirgen H, Levy EK. Analytical modeling of water condensation in condensing heat exchanger. *Int J Heat Mass Transfer*. 2010;53:2361–2368.
14. Schrock VE, Grossman LM. Forced convection boiling in tubes. *Nucl Sci Eng*. 1962;12:474–481.
15. Wojtan L, Ursenbacher T, Thome JR. Investigation of flow boiling in horizontal tubes: part I—a new diabatic two-phase flow pattern map. I. *J Heat Mass Transfer*. 2005;48:2955–2969.
16. Wojtan L, Ursenbacher T, Thome JR. Investigation of flow boiling in horizontal tubes: part II—development of a new heat transfer model for stratified-wavy, dryout and mist flow regimes. I. *J Heat Mass Transfer*. 2005;48:2970–2985.
17. Mori H, Yoshida S, Ohishi K, Kokimoto Y. Dryout quality and post dryout heat transfer coefficient in horizontal evaporator tubes. In: Proceedings of the 3rd European Thermal Sciences Conference. Heidelberg, Germany: Eurotherm (editor and publisher). 2000:839–844.
18. Colburn AP. A method of correlating forced convection heat transfer data and a comparison with fluid friction. *Trans Am Inst Chem Eng*. 1933;29:174–210.
19. Chilton TH, Colburn AP. Mass transfer (adsorption) coefficients: prediction from data on heat transfer and fluid friction. *Ind Eng Chem*. 1934;26:1183–1187.
20. Stephan K. *Heat Transfer in Condensation and Boiling*. New York: Springer-Verlag, 1992.
21. Incropera FP, Dewitt DP, Bergman TL, Lavine AS. *Fundamentals of Heat and Mass Transfer*, 6th ed. Hoboken, NJ: Wiley, 2007.
22. Zhukauskas AA. Heat Transfer from Tubes in Cross Flow. *Adv Heat Transfer*. 1972;8:93–160.
23. Gnielinski V. New equations for heat and mass transfer in turbulent pipe and channel flow. *Int Chem Eng*. 1976;16:359–368.
24. Morooka S, Inai N, Tobimatsu T. Experimental investigation of heat transfer in BWR LOCA. *J Nucl Sci Technol*. 1981;18:473–475.
25. Thermophysical Properties of Fluid Systems. NIST. Available at: http://webbook.nist.gov/chemistry/fluid/.

Manuscript received July 2, 2010, and revision received Dec. 3, 2010.